

pubs.acs.org/JPCA Article

Ab Initio Approach to Femtosecond Stimulated Raman Spectroscopy: Investigating Vibrational Modes Probed in Excited-State Relaxation of Quaterthiophenes

Saswata Dasgupta and John M. Herbert*



Cite This: J. Phys. Chem. A 2020, 124, 6356-6362



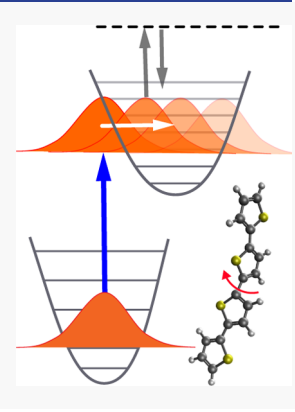
ACCESS

III Metrics & More



Supporting Information

ABSTRACT: Femtosecond stimulated Raman spectroscopy (FSRS) is an ultrafast pump—probe technique designed to elucidate excited-state molecular dynamics by means of vibrational spectroscopy. We present a first-principles protocol for the simulation of FSRS that integrates *ab initio* molecular dynamics with computational resonance Raman spectroscopy. Theoretical calculations can monitor the time-dependent evolution of specific vibrational modes and thus provide insight into the nature of the motion responsible for the experimental FSRS signal, and we apply this technique to study quaterthiophene derivatives. The S₁ state of two different quaterthiophene derivatives relaxes via inphase and out-of-phase stretching modes whose frequencies are coupled to the dihedral backbone angle, such that the spectral evolution reflects the excited-state relaxation toward a planar conformation. The simulated spectra aid in confirming the experimental assignment of the vibrational modes that are probed in the existing FSRS experiments on quaterthiophenes.



1. INTRODUCTION

Interrogation of bond-breaking and bond-forming processes with femtosecond time resolution is a central goal of experimental chemical dynamics. Femtosecond stimulated Raman spectroscopy (FSRS) has emerged as a powerful technique offering both temporal and spectral resolution, 1-3 which can therefore be used to provide real-time information on structural changes as a photochemical reaction proceeds on an excited-state potential energy surface.3-5 By means of femtosecond dynamic absorption spectroscopy, 6,7 the FSRS technique sidesteps the transform-limited time-energy uncertainty relationship and can provide a time resolution of \lesssim 50 fs in tandem with a frequency resolution of <10 cm⁻¹. ¹⁻³ FSRS is a four-wave mixing experiment, or a six-wave mixing experiment in the presence of an actinic pump pulse, in which the actinic pump pulse promotes the system to an excited electronic state and thereby initiates a photochemical event. A subsequent combination of a narrowband (picosecond) Raman pump pulse, which determines the frequency resolution, with a femtosecond probe pulse affords time-resolved vibrational spectra of transient electronic states.¹⁻³ In the present work, we present an ab initio simulation protocol for FSRS and use this approach to examine the relaxation dynamics in the S₁ state of quaterthiophene derivatives, by means of resonantly enhanced FSRS based on the $S_1 \rightarrow S_2$ transition.

Photophysical processes in conjugated organic polymers have been the subject of considerable scrutiny because of the utility of these materials as organic photovoltaics. ^{10–12} Timeresolved electronic spectroscopy of these materials has been used to probe the dynamics of excitonic charge carriers, ^{13–16}

revealing the relaxation dynamics on (sub-)picosecond time-scales, 13,16 but time-resolved, resonance-enhanced Raman spectroscopy can characterize the minute details of the excited-state dynamics with vibrational specificity. 17,18 Raman spectroscopy can also be used to examine the extent of π delocalization in conjugated oligomers. $^{19-21}$ To this end, Bragg and co-workers 22 used resonance-enhanced FSRS to study the conformational relaxation of the photoexcited S_1 state of 2,2':5',2"'-quaterthiophene (4T, Figure 1a) and 3,3"'-dihexyl-2,2':5',2"'-quaterthiophene (DH4T) in chlorobenzene solution.

The experimental spectra of 4T and DH4T (Figure 2) display three major features: 22 (i) C–S–C ring deformation at vibrational wavenumbers <700 cm $^{-1}$; (ii) prominent intensities for in-phase C=C stretch (" Π " mode in Figure 2) and out-of-phase C=C stretch (" Π " mode), for both molecules; and (iii) relative intensities for the Π and Π features being reversed in 4T versus DH4T. These experiments have established that the intensity ratio

$$ROI = \frac{I(\mathfrak{R})}{I(Z)} \tag{1}$$

Received: July 9, 2020 Published: July 14, 2020





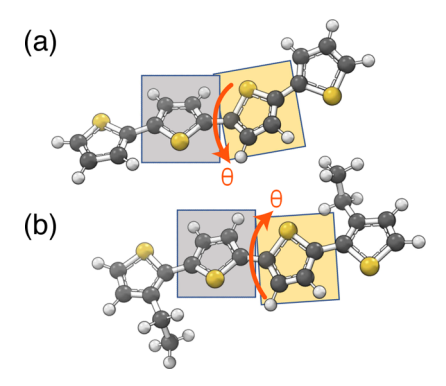


Figure 1. Structures of the two quaterthiophene molecules considered in this work: (a) 4T and (b) DE4T. The primary geometric parameter of interest is the dihedral angle θ between the indicated planes, containing the two central thiophene units. Ground-state geometries are shown, which are distorted away from the planar all-trans thiophene backbone (at $\theta = 180^{\circ}$) that represents the S₁ minimum-energy geometry (Figure S1). A secondary minimum in the S₁ state (trans-cis geometry at $\theta = 0$) is only slightly higher in energy; see Figure S2.

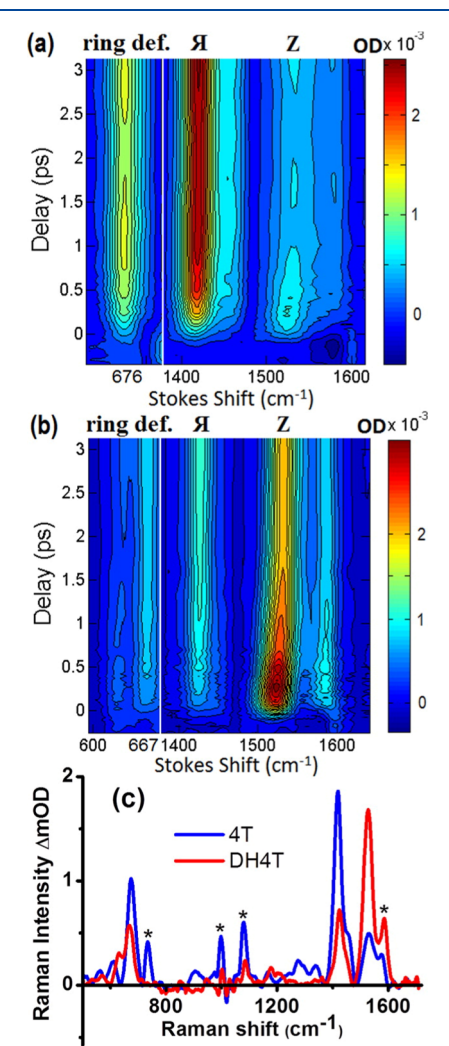


Figure 2. FSRS spectra of (a) 4T and (b) DH4T in chlorobenzene, following photoexcitation at 350 nm. The in-phase (Я) and out-of-phase (Z) intra-ring C=C frequencies are labeled. (c) One-dimensional slices of the spectra obtained 2 ps after photoexcitation. Adapted from ref 22; copyright 2015 American Chemical Society.

between the in-phase and out-of-phase C=C modes is a manifestation of motion along the dihedral angle between the central thiophene blocks; see Figure 1. The ratio ROI in eq 1 is thought to report on the S_1 relaxation process, as the quaterthiophene with the more bulky substituent relaxes faster as a result of steric repulsion between the alkyl side chain and the adjacent thiophene ring. $^{21-23}$

That said, most computational efforts to rationalize FSRS experiments have so far relied on ground- and excited-state vibrational frequency and Raman intensity calculations, ^{21,22} or else off-resonant calculations. ²⁴ There have been only a few previous efforts at the direct simulation of the stimulated Raman signal itself, on the basis of *ab initio* molecular dynamics (*ai*MD). ^{25,26} The direct simulation of FSRS using *ab initio* quantum chemistry, as pursued in the present work, may aid in making mode assignments.

2. COMPUTATIONAL DETAILS

In the present study, we consider 3,3"'-diethyl-2,2':5',2":5",2"'-quaterthiophene (DE4T, Figure 1b) rather than DH4T. The ground states of all the three molecules (4T, DE4T, and DH4T) are characterized by a nonplanar thiophene backbone, which is distorted away from the all-trans geometry that represents the S₁ minimum. (Optimized geometries for both the S₀ and S₁ states of 4T and DE4T are depicted in Figure S1.) Following S₀ \rightarrow S₁ excitation, relaxation occurs along the interior dihedral angle θ that is suggested in Figure 1, leading to either the all-trans structure (S₁ global minimum) with θ = 180° or else a slightly higher-energy trans—cis structure with θ = 0. Potential energy scans $V(\theta)$ for the S₁ state of 4T and DE4T can be found in Figure S2.

The experiments reported in ref 22 used an 850 nm probe laser (photon energy of 1.46 eV) for 4T and 880 nm (1.41 eV) for D4HT, for resonant excitation of molecules that were first pumped to the S_1 state. To ascertain which S_n state is excited by the probe laser, we computed vertical excitation energies for the $S_1 \rightarrow S_n$ transitions (n = 2, 3, 4) at the minimum-energy geometry on the S_1 state. These values are reported in Table 1.

Table 1. Vertical Excitation Energies (in eV) Computed at the S_1 Minimum-Energy Geometry^a

	$TD ext{-}DFT^b$		$SOS-CIS(D)^c$	
transition	4T	DE4T	4T	DE4T
$S_1 \rightarrow S_2$	1.27	1.21	1.31	1.42
$S_1 \rightarrow S_3$	1.41	1.43	2.05	2.47
$S_1 \rightarrow S_4$	1.95	1.88	2.38	2.50

^aBased on the differences in $S_0 \rightarrow S_n$ excitation energies at the CAM-B3LYP/6-31++G* geometry of the S_1 state. ^bCAM-B3LYP/6-31G*. ^cSOS-CIS(D)/6-31++G*.

Calculations were performed using time-dependent density functional theory (TD-DFT) at the CAM-B3LYP/6-31G* level, 27 an affordable approach that will be used for the aiMD simulations that are reported below, and also using a correlated wave function method: scaled opposite spin (SOS) configuration interaction singles with perturbative doubles [CIS-(D)]. We consider the SOS-CIS(D) approach to be the more reliable method for computing vertical excitation energies, and the $S_1 \rightarrow S_n$ transition energies computed at that level of theory suggest that only the S_2 state is accessible at the experimental probe wavelengths. For this reason, we assume that the experimental measurement is resonantly

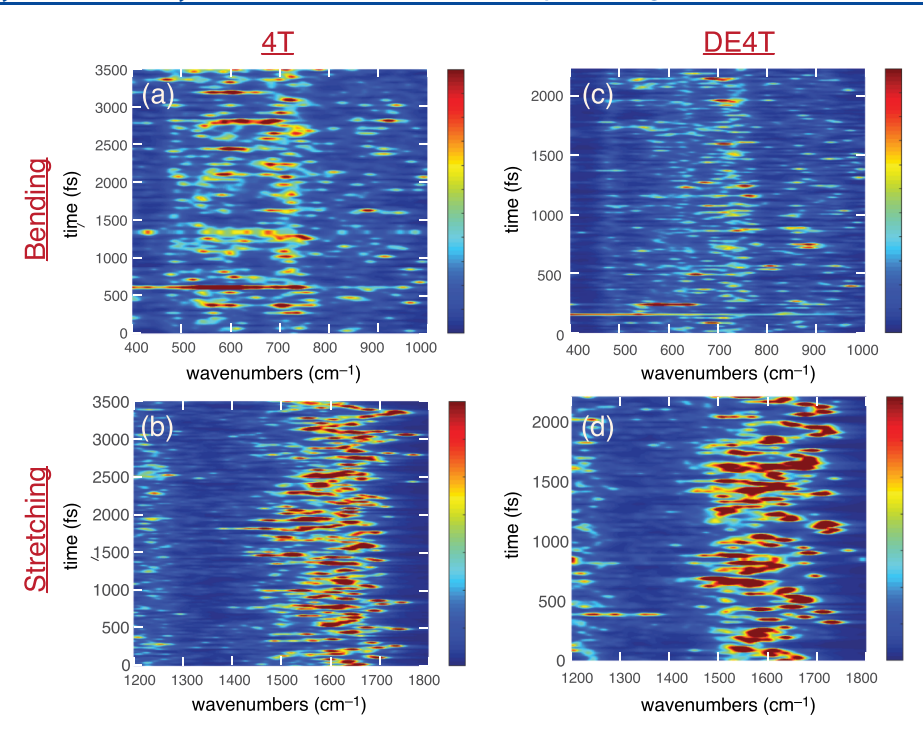


Figure 3. Time-evolving, excited-state $(S_1 \rightarrow S_2)$ RR intensities computed from TD-DFT trajectories in the S_1 state of 4T (left) and DE4T (right). The color bar quantifies relative intensity enhancements and is therefore dimensionless.

enhanced by $S_1 \rightarrow S_2$ excitation. (This transition is characterized by the incipient formation of double bonds between the central and the peripheral thiophene rings, as shown in Figure S3.) The assumption that the molecule is promoted to S_2 is validated below by also computing the FSRS signal under the alternative assumption of $S_1 \rightarrow S_3$ enhancement, for which we obtain far less good agreement with the experimental spectra in Figure 2.

These FSRS signals are computed by means of aiMD simulations in the S_1 state, for a 4T or DE4T molecule initially excited from the all-trans S_0 geometry. These simulations were performed using TD-DFT at the CAM-B3LYP/6-31G* level, ²⁷ for which the $S_1 \rightarrow S_2$ transition energy is only slightly lower than the SOS-CIS(D) estimate (Table 1) but where affordable analytic gradients are available in order to propagate trajectories on excited-state potential surfaces. Resonance Raman (RR) intensities, corresponding to the $S_1 \rightarrow S_2$ electronic transition except where otherwise indicated, were computed at 10 fs intervals along the S_1 trajectory, according to the formula 30,31

$$I_k \propto \omega_{\rm L}(\omega_{\rm L} - \omega_k)^3 (\omega_k \Delta_k)^2$$
 (2)

which comes from the excited-state gradient (short-time) approximation, equivalent to the independent-mode displaced harmonic oscillator (IMDHO) model. $^{30-36}$ In eq 2, ω_k is the frequency of the kth normal mode in the initial (S₁) state and Δ_k is the dimensionless displacement of the kth normal mode between the initial and final states. The quantity ω_L in eq 2 is the laser frequency, which would be necessary to compute absolute RR intensities but which cancels in the excited-state formalism that is described in more detail below. Within this approach, what is required are initial-state frequencies ω_k but only single-point gradient calculations on the final state, in order to obtain the displacement Δ_k .

Simulations were performed at T = 300 K using a Nosé–Hoover thermostat. Following equilibration on the ground

state, the total S_1 simulation time was 3.5 ps for 4T and 2.2 ps for DE4T, using a time step of 0.6 fs. All calculations were performed using Q-Chem v. 5.3,³⁷ in which the RR formalism was recently implemented by the present authors.³¹ All excited-state calculations (including vibrational frequencies) were performed using TD-DFT at the CAM-B3LYP/6-31G* level using the SG-1 quadrature grid.³⁸

3. RESULTS AND DISCUSSION

Excited-state RR profiles, computed as a function of time along the S₁ trajectory, serve as proxies for the FSRS signal, and these time-dependent RR profiles for 4T and DE4T are plotted in Figure 3. The spectra in the ring deformation (bending) region qualitatively reproduce the experimental observations shown in Figure 2, insofar as 4T exhibits an intense band between 500 and 700 cm⁻¹, whereas the spectrum of DE4T is quite weak in the same region. For comparison, we have also computed the time-evolving RR intensities under the assumption of resonant enhancement via $S_1 \rightarrow S_3$ excitation; see Figure S4. Compared to the spectra in Figure 3, $S_1 \rightarrow S_3$ excitation lights up not only the in-phase and out-of-phase C=C vibrations but numerous other modes as well, leading to a spectrum that seems to contain more features than the experimental spectrum. This, combined with the SOS-CIS(D) excitation energies that seem to preclude $S_1 \rightarrow S_3$ excitation at the experimental probe wavelengths (as discussed above), led us to consider only $S_1 \rightarrow$ S₂ excitation in what follows.

Although our computed RR spectra for both 4T and DE4T exhibit intense bands in the C=C stretching region, the peaks are difficult to resolve. These time-dependent RR profiles turn out to be rather crude proxies for the FSRS signal, and it is necessary to go beyond this simple approach. The resolution problems ultimately stem from the use of an instantaneous normal mode (INM) formalism, ³⁹ in which the excited-state frequencies ω_k are computed at nonstationary geometries along an aiMD trajectory. This approach is known to produce

oscillatory vibrational frequency profiles, 25,40 due to the of the nonvanishing time-dependent gradient, $\mathbf{g}(t)$, which may be rectified through the use of a time-integrated Hessian.

Let $\mathbf{Q}(t)$ denote the INM coordinates obtained by diagonalizing the instantaneous Hessian matrix, $\mathbf{H}(t)$. The S_1 potential surface has a local expansion in the coordinates $\mathbf{Q}(t)$, centered at $\mathbf{Q} = \mathbf{0}$ and having the form

$$V(\mathbf{Q}, t) \approx V_0 + \mathbf{g}(t)^{\dagger} \mathbf{Q}(t) + \frac{1}{2} \mathbf{Q}(t)^{\dagger} \mathbf{H}(t) \mathbf{Q}(t)$$
(3)

where $V_0 = V(\mathbf{0})$. To sidestep the oscillations engendered by the nonzero gradient, Li and co-workers suggest averaging the fluctuating potential energy over a fixed time interval, τ : ^{25,40}

$$\overline{V}(t) = \frac{1}{\tau} \int_{t-\tau/2}^{t+\tau/2} V(t') \, dt'$$
 (4)

Time-averaging the gradient and the Hessian in the same way,

$$\overline{\mathbf{g}}(t) = \frac{1}{\tau} \int_{t-\tau/2}^{t+\tau/2} \mathbf{g}(t') \, \mathrm{d}t' \tag{5a}$$

$$\bar{\mathbf{H}}(t) = \frac{1}{\tau} \int_{t-\tau/2}^{t+\tau/2} \mathbf{H}(t') \, \mathrm{d}t'$$
 (Sb)

affords a time-averaged local expansion of the potential energy surface:

$$\overline{V}(\mathbf{Q}, t) = \overline{V}(t) + \overline{\mathbf{g}}(t)^{\dagger} \mathbf{Q}(t) + \frac{1}{2} \mathbf{Q}(t)^{\dagger} \overline{\mathbf{H}}(t) \mathbf{Q}(t)$$
(6)

If τ is chosen to be the fundamental vibrational period for a particular (rapidly varying) coordinate, then one may anticipate that $\mathbf{g}(t)$ averages approximately to zero in eq 5a, as it does for a simple harmonic oscillator. If $\overline{\mathbf{g}}(t) \approx \mathbf{0}$, then the time-averaged quadratic potential energy function becomes

$$\overline{V}(\mathbf{Q}, t) \approx \overline{V}(t) + \frac{1}{2}\mathbf{Q}(t)^{\dagger}\overline{\mathbf{H}}(t)\mathbf{Q}(t)$$
 (7)

analogous to the case of vibrational frequency analysis at a stationary geometry. In practice, we take the normal modes $\mathbf{Q}(t)$ to be the instantaneous eigenvectors of $\overline{\mathbf{H}}(t)$ rather than $\mathbf{H}(t)$. By time-averaging the Hessian prior to diagonalization, one may preserve information about couplings between normal modes that might be lost if one simply averaged the instantaneous INM frequency.

The utility of this averaging procedure can be understood using a simple example of a vibrationally hot H₂ molecule, at T = 423 K in its ground electronic state. Instantaneous frequency profiles, obtained by diagonalizing either $\mathbf{H}(t)$ or $\overline{\mathbf{H}}(t)$ along a ground-state DFT trajectory, are shown in Figure 4. Although the molecule does not undergo any photochemical process, the nonzero gradient nevertheless results in large fluctuations in the INM frequency, which oscillates rapidly over a range from 3600 to 5200 cm⁻¹. Time-averaging significantly dampens these fluctuations, and a much more consistent vibrational frequency emerges. Figure S5 shows the effect of averaging on the time-evolving frequency profile of H₂ when the intensity includes the Δ_k factor from eq 2. Although the INM spectrum is scattered and diffuse, as seen also in Figure 3, time-averaging allows one to easily follow the time-evolving vibrational frequency.

For large molecules whose vibrational motions span a range of timescales, time-averaging every mode with a different time window τ would be quite complicated. Instead, time-averaging

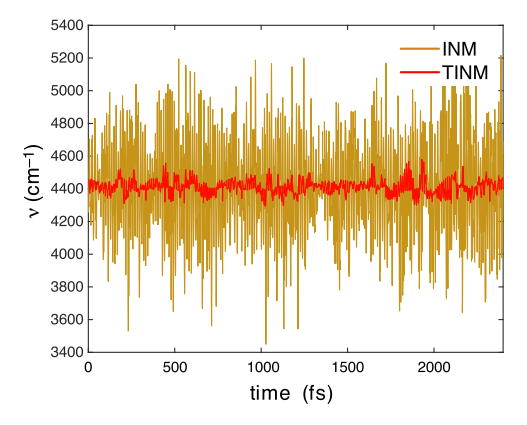


Figure 4. Instantaneous frequency profile for ground-state H_2 at T = 423 K, obtained within the INM approach as the eigenvalues of $\mathbf{H}(t)$, or else within the time-averaged INM approach as the eigenvalues of $\mathbf{\bar{H}}(t)$. Calculations were performed at the B3LYP/6-31G* level.

should be performed for the modes that are tough to resolve spectroscopically. For the quaterthiophenes considered here, we use a window $\tau = 20$ fs in eq 5b, corresponding to $\tilde{\nu} = 1670$ cm⁻¹. This lies in the range of the C=C modes of interest.

We compute the resonantly enhanced FSRS signal using RR intensity ratios

$$\frac{I_j(t)}{I_k(t)} = \left(\frac{\omega_j(t)\Delta_j(t)}{\omega_k(t)\Delta_k(t)}\right)^2 \tag{8}$$

for the relative intensity of normal modes Q_j and Q_k .³¹ Here, the frequencies $\omega_j(t)$ and $\omega_k(t)$ are taken to be instantaneous eigenvalues of the time-integrated Hessian $\overline{\mathbf{H}}(t)$. Within the IMDHO picture, the quantities Δ_j and Δ_k are the displacements (between initial and final electronic states) of the minimum-energy geometry along the modes Q_j and Q_k . As in a previous work, these can be computed from the gradient $\partial\Omega/\partial\mathbf{Q}$ of the electronic transition energy, Ω :

$$\Delta_k = -\frac{1}{\sqrt{\hbar\omega_k^3}} \left(\frac{\partial \Omega}{\partial Q_k} \right) \bigg|_{\mathbf{Q} = \mathbf{0}} \tag{9}$$

Note that Δ_k is a signed quantity that carries information regarding the equilibrium position of the upper state with respect to the lower state.⁴¹ For resonant enhancement using the $S_1 \rightarrow S_2$ transition, the calculation of $\partial \Omega/\partial Q_k$ requires two TD-DFT gradient calculations at each time step, one for the S_1 state and one for S_2 .

In the previous INM calculations (Figure 3), the in-phase and out-of-phase modes were difficult to resolve, so in the absence of a great deal of previous work on these molecules, *a priori* assignment of the vibrational modes responsible for the FSRS signal would have been quite challenging. The time-averaged approach, in contrast, affords two well-resolved bands in the C=C stretch region, as seen in Figure 5. Mode assignment is therefore unambiguous, although the peaks are not sharp enough to compute the intensity ratio, that is, ROI in eq 1. Nevertheless, integration of the excited-state RR spectra with the *ai*MD simulation successfully describes the bright band in the ring deformation region, observed for 4T (Figure 3a) but which is absent in DE4T (Figure 3b).

To address the intensity ratio, we computed RR intensities for the $S_1 \rightarrow S_2$ transition at optimized geometries on the S_1 surfaces of 4T and DE4T, constraining the dihedral angle θ in

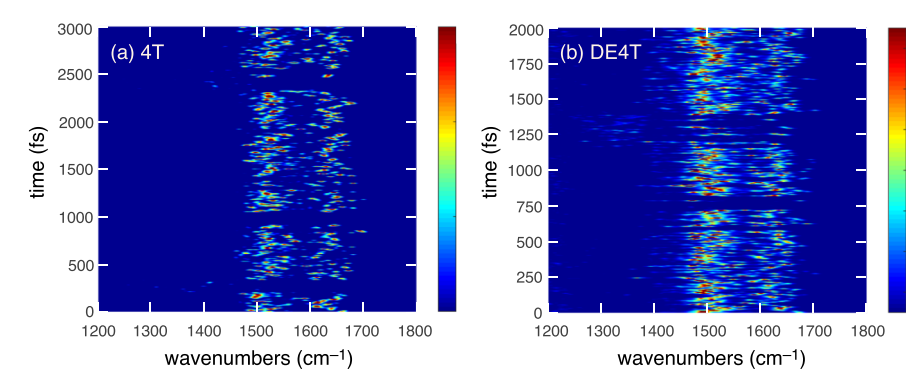


Figure 5. Time-integrated excited-state RR spectra ($S_1 \rightarrow S_2$ transition) obtained from *aiMD* trajectories on the S_1 state of (a) 4T and (b) DE4T, obtained by diagonalizing the time-averaged Hessian $\overline{\mathbf{H}}(t)$ over an interval $\tau = 20$ fs. Intensities come from the enhancement ratio defined in eq 8, and the units are therefore arbitrary, hence, the color bar that defines the relative spectral intensity is dimensionless.

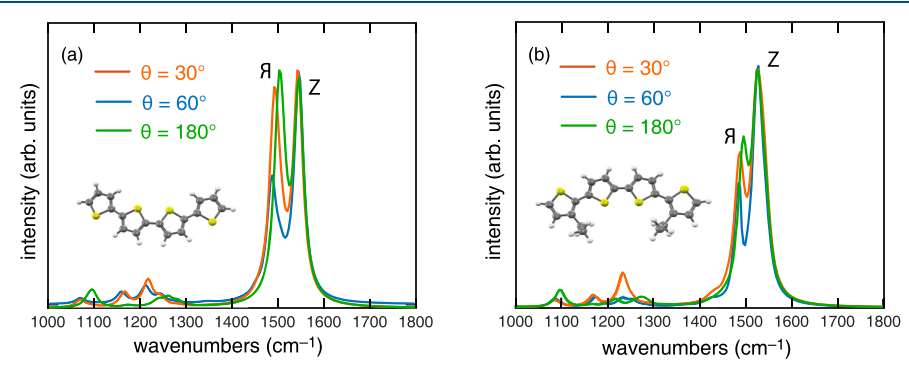


Figure 6. Stationary RR spectra ($S_1 \rightarrow S_2$ transition) for (a) 4T and (b) DE4T, computed at geometries optimized on the S_1 state. The fully relaxed (minimum-energy S_1) geometries correspond to a torsion angle $\theta = 180^\circ$. Also shown are the RR spectra computed for constrained values $\theta = 30^\circ$ and $\theta = 60^\circ$, with all remaining coordinates relaxed on the S_1 state. Calculations were performed at the CAM-B3LYP/6-31G* level.

 30° increments between $\theta = 0$ and $\theta = 180^{\circ}$, with all other degrees of freedom relaxed on the S_1 surface. The whole series of spectra can be found in Figure S6, and a subset of them is shown in Figure 6. The dependence of ROI on θ is clearly evident, as this intensity ratio increases with the increasing loss of planarity starting from the minimum-energy S₁ geometry at $\theta = 180^{\circ}$. Higher intensity is obtained for the in-phase mode (\mathfrak{R}) in the case of 4T, as compared to the out-of-phase mode (Z); however, the pattern is reversed for DE4T, resulting in a much larger value of ROI. Because previous computational work suggests that RR intensities computed using TD-DFT may be sensitive to the choice of functional,³ confirmed that calculations using B3LYP and PBE0 also predict a larger ROI for DE4T, in agreement with the CAM-B3LYP results in Figure 6. (Results with these other two functionals are provided in Figure S7.)

In FSRS experiments on quaterthiophenes, an increase in ROI is interpreted as evidence for twisting away from a planar structure. To examine this, we optimized the S_1 geometries of 4T and DE4T subject to a constraint on the central dihedral torsion angle θ , relaxing all other coordinates. Changes in the ROI observed in the RR spectra at constrained dihedral angles suggest that this ratio is indeed enhanced when the geometry is nonplanar. The time-dependent evolution of θ along excited-state trajectories (Figure S8) sheds light on the role of the steric effect on the dynamics in the S_1 state. In DE4T, this angle evolves on the S_1 state to a value that is farther from 180° (i.e., farther from the planar structure) than it does in 4T. This reinforces conclusions drawn from examining the intensity ratio ROI, namely, that steric hindrance in DE4T leads to

faster torsional dynamics as compared to its unsubstituted counterpart.

4. CONCLUSIONS

We have introduced a protocol for first-principles simulation of FSRS based on excited-state aiMD trajectories. Instantaneous, time-evolving RR spectra computed on the excited state provide snapshots to explain the spectral dynamics and facilitate mode assignments. A time-integrated normal mode procedure sidesteps problems with INM calculations, that is, with vibrational "frequencies" computed at nonstationary geometries. For FSRS experiments that probe dynamics through a conical intersection, 42 nonadiabatic aiMD algorithms will be required, 43-46 for example, based on trajectory surface hopping. 47,48 The ab initio nature of the present approach to FSRS should be integrable with these nonadiabatic aiMD algorithms. For reactive FSRS, experiments have emphasized the role of anharmonic couplings, 42 for which the excited-state gradient formalism that is used herein to compute RR intensity enhancements would need to be replaced by a more general formalism based on derivatives of the polarizability tensor.³⁶ This might also be helpful for resolving experimental ambiguities regarding signals arising from lower-order nonlinear processes, which complicate the analysis of FSRS spectra.9 These are interesting avenues for future work.

ASSOCIATED CONTENT

Supporting Information

The Supporting Information is available free of charge at https://pubs.acs.org/doi/10.1021/acs.jpca.0c06307.

Additional spectra and supporting calculations (PDF) Constrained optimized geometries for 4T and DE4T-(TXT)

AUTHOR INFORMATION

Corresponding Author

John M. Herbert — Department of Chemistry and Biochemistry, The Ohio State University, Columbus, Ohio 43210, United States; ⊚ orcid.org/0000-0002-1663-2278; Email: herbert@ chemistry.ohio-state.edu

Author

Saswata Dasgupta — Department of Chemistry and Biochemistry, The Ohio State University, Columbus, Ohio 43210, United States; orcid.org/0000-0002-8014-8376

Complete contact information is available at: https://pubs.acs.org/10.1021/acs.jpca.0c06307

Notes

The authors declare the following competing financial interest(s): J.M.H. serves on the board of directors of Q-Chem Inc.

ACKNOWLEDGMENTS

This work was supported by National Science Foundation grant no. CHE-1665322, and calculations were performed at the Ohio Supercomputer Center under project PAA-0003.⁴⁹

■ REFERENCES

- (1) McCamant, D. W.; Kukura, P.; Yoon, S.; Mathies, R. A. Femtosecond broadband stimulated Raman spectroscopy: Apparatus and methods. *Rev. Sci. Instrum.* **2004**, *75*, 4971–4980.
- (2) Dietze, D. R.; Mathies, R. A. Femtosecond stimulated Raman spectroscopy. *ChemPhysChem* **2016**, *17*, 1224–1251.
- (3) Kukura, P.; McCamant, D. W.; Mathies, R. A. Femtosecond stimulated Raman spectroscopy. *Annu. Rev. Phys. Chem.* **2007**, *58*, 461–488.
- (4) McCamant, D. W.; Kukura, P.; Mathies, R. A. Femtosecond time-resolved stimulated Raman spectroscopy: Application to the ultrafast internal conversion in β -carotene. *J. Phys. Chem. A* **2003**, *107*, 8208–8214.
- (5) Laimgruber, S.; Schreier, W. J.; Schrader, T.; Koller, F.; Zinth, W.; Gilch, P. The photochemistry of *o*-nitrobenzaldehyde as seen by femtosecond vibrational spectroscopy. *Angew. Chem., Int. Ed.* **2005**, 44, 7901–7904.
- (6) Pollard, W. T.; Mathies, R. A. Analysis of femtosecond dynamic absorption spectra of nonstationary states. *Annu. Rev. Phys. Chem.* **1992**, 43, 497–523.
- (7) Lee, S.-Y.; Zhang, D.; McCamant, D. W.; Kukura, P.; Mathies, R. A. Theory of femtosecond stimulated Raman spectroscopy. *J. Chem. Phys.* **2004**, *121*, 3632–3642.
- (8) Sun, Z.; Lu, J.; Zhang, D. H.; Lee, S.-Y. Quantum theory of (femtosecond) time-resolved stimulated Raman scattering. *J. Chem. Phys.* **2008**, *128*, 144114.
- (9) Molesky, B. P.; Guo, Z.; Moran, A. M. Femtosecond stimulated Raman spectroscopy by six-wave mixing. *J. Chem. Phys.* **2015**, *142*, 212405.
- (10) Günes, S.; Neugebauer, H.; Sariciftci, N. S. Conjugated polymer-based organic solar cells. *Chem. Rev.* **2007**, *107*, 1324–1338. (11) Facchetti, A. π-Conjugated polymers for organic electronics and photovoltaic cell applications. *Chem. Mater.* **2011**, *23*, 733–758.

- (12) Ostroverkhova, O. Organic optoelectronic materials: Mechanisms and applications. *Chem. Rev.* **2016**, *116*, 13279–13412.
- (13) Lanzani, G.; Nisoli, M.; Magni, V.; De Silvestri, S.; Barbarella, G.; Zambianchi, M.; Tubino, R. Femtosecond spectral relaxation of α -conjugated hexamethylsexithiophene in solution. *Phys. Rev. B: Condens. Matter Mater. Phys.* **1995**, *51*, 13770–13773.
- (14) Lanzani, G.; Nisoli, M.; De Silvestri, S.; Tubino, R. Femtosecond vibrational and torsional energy redistribution in photoexcited oligothiophenes. *Chem. Phys. Lett.* **1996**, *251*, 339–345.
- (15) Clark, J.; Nelson, T.; Tretiak, S.; Cirmi, G.; Lanzani, G. Femtosecond torsional relaxation. *Nat. Phys.* **2012**, *8*, 225–231.
- (16) Kim, P.; Park, K. H.; Kim, W.; Tamachi, T.; Iyoda, M.; Kim, D. Relationship between dynamic planarization processes and exciton delocalization in cyclic oligothiophenes. *J. Phys. Chem. Lett.* **2015**, *6*, 451–456.
- (17) Yamaguchi, S.; Hamaguchi, H.-o. Ultrafast vibrational relaxation in photogenerated S_1 α -terthiophene in solution by femtosecond time-resolved absorption/emission and picosecond time-resolved Raman spectroscopy. *Chem. Phys. Lett.* **1994**, 227, 255–260.
- (18) Iwata, K.; Hamaguchi, H.-o. Picosecond time-resolved Raman spectroscopy of S_1 p-terphenyl and p-terphenyl- d_{14} in solution: Time-dependent changes of Raman band shapes. *J. Raman Spectrosc.* **1994**, 25, 615–621.
- (19) Castiglioni, C.; Del Zoppo, M.; Zerbi, G. Vibrational Raman spectroscopy of polyconjugated organic oligomers and polymers. *J. Raman Spectrosc.* **1993**, *24*, 485–494.
- (20) Hernandez, V.; Castiglioni, C.; Del Zoppo, M.; Zerbi, G. Confinement potential and π -electron delocalization in polyconjugated organic materials. *Phys. Rev. B: Condens. Matter Mater. Phys.* **1994**, 50, 9815–9823.
- (21) Donohoo-Vallett, P. J.; Bragg, A. E. π -Delocalization and the vibrational spectroscopy of conjugated materials: Computational insights on Raman frequency dispersion in thiophene, furan, and pyrrole oligomers. *J. Phys. Chem. B* **2015**, *119*, 3583–3594.
- (22) Zhou, J.; Yu, W.; Bragg, A. E. Structural relaxation of photoexcited quaterthiophenes probed with vibrational specificity. *J. Phys. Chem. Lett.* **2015**, *6*, 3496–3502.
- (23) Yu, W.; Donohoo-Vallett, P. J.; Zhou, J.; Bragg, A. E. Ultrafast photo-induced nuclear relaxation of a conformationally disordered conjugated polymer probed with transient absorption and femtosecond stimulated Raman spectroscopies. *J. Chem. Phys.* **2014**, *141*, 044201.
- (24) Barclay, M. S.; Quincy, T. J.; Williams-Young, D. B.; Caricato, M.; Elles, C. G. Accurate assignments of excited-state resonance Raman spectra: A benchmark study combining experiment and theory. J. Phys. Chem. A 2017, 121, 7937—7946.
- (25) Petrone, A.; Williams-Young, D. B.; Lingerfelt, D. B.; Li, X. Ab initio excited-state transient Raman analysis. *J. Phys. Chem. A* **2017**, 121, 3958–3965.
- (26) Chiariello, M. G.; Rega, N. Exploring nuclear photorelaxation of pyranine in aqueous solution: An integrated ab-initio molecular dyanmics and time resolved vibrational analysis approach. *J. Phys. Chem. A* **2018**, *122*, 2884–2893.
- (27) Yanai, T.; Tew, D. P.; Handy, N. C. A new hybrid exchange-correlation functional using the Coulomb-attenuating method (CAM-B3LYP). *Chem. Phys. Lett.* **2004**, 393, 51–57.
- (28) Rhee, Y. M.; Head-Gordon, M. Scaled second-order perturbation corrections to configuration interaction singles: Efficient and reliable excitation energy methods. *J. Phys. Chem. A* **2007**, *111*, 5314–5326.
- (29) Loos, P. F.; Jacquemin, D. Evaluating 0-0 energies with theoretical tools: A short review. *ChemPhotoChem* **2019**, *3*, 684-696.
- (30) Jarzęcki, A. A. Quantum-mechanical calculations of resonance Raman intensities: The weighted-gradient approximation. *J. Phys. Chem. A* **2009**, *113*, 2926–2934.
- (31) Dasgupta, S.; Rana, B.; Herbert, J. M. *Ab initio* investigation of the resonance Raman spectrum of the hydrated electron. *J. Phys. Chem. B* **2019**, *123*, 8074–8085.

- (32) Kane, K. A.; Jensen, L. Calculation of absolute resonance Raman intensities: Vibronic theory vs short-time approximation. *J. Phys. Chem. C* **2010**, *114*, 5540–5546.
- (33) Petrenko, T.; Neese, F. Efficient and automatic calculation of optical band shapes and resonance Raman spectra for larger molecules within the independent mode displaced harmonic oscillator model. *J. Chem. Phys.* **2012**, *137*, 234107.
- (34) Silverstein, D. W.; Govind, N.; van Dam, H. J. J.; Jensen, L. Simulating one-photon absorption and resonance Raman scattering spectra using analytical excited state energy gradients within time-dependent density functional theory. *J. Chem. Theory Comput.* **2013**, 9, 5490–5503.
- (35) Guthmuller, J. Comparison of simplified sum-over-state expressions to calculation resonance Raman intensities including Franck-Condon and Herzberg-Teller effects. J. Chem. Phys. 2016, 144, 064106
- (36) Guthmuller, J. Calculation of vibrational resonance Raman spectra of molecules using quantum chemistry methods. In *Molecular Spectroscopy: A Quantum Chemistry Approach*; Ozaki, Y., Wójcik, M. J., Popp, J., Eds.; Wiley-VCH: Weinheim, Germany, 2019; Vol. 1, Chapter 17, pp 497–536.
- (37) Shao, Y.; et al. Advances in molecular quantum chemistry contained in the Q-Chem 4 program package. *Mol. Phys.* **2015**, *113*, 184–215.
- (38) Gill, P. M. W.; Johnson, B. G.; Pople, J. A. A standard grid for density-functional calculations. *Chem. Phys. Lett.* **1993**, 209, 506–512.
- (39) Stratt, R. M. The instantaneous normal modes of liquids. *Acc. Chem. Res.* **1995**, 28, 201–207.
- (40) Petrone, A.; Lingerfelt, D. B.; Williams-Young, D. B.; Li, X. Ab initio transient vibrational spectral analysis. *J. Phys. Chem. Lett.* **2016**, 7, 4501–4508.
- (41) Zink, J. I.; Shin, K.-S. K. Molecular distortions in excited electronic states determined from electronic and resonance Raman spectroscopy. In *Advances in Photochemistry*; Volman, D. H., Hammond, G. S., Neckers, D. C., Eds.; John Wiley & Sons: New York, 1991; Vol. 16, Chapter 3, pp 119–214.
- (42) Hoffman, D. P.; Mathies, R. A. Femtosecond stimulated Raman exposes the role of vibrational coherence in condensed-phase photoreactivity. *Acc. Chem. Res.* **2016**, *49*, 616–625.
- (43) Subotnik, J. E.; Alguire, E. C.; Ou, Q.; Landry, B. R.; Fatehi, S. The requisite electronic structure theory to describe photoexcited nonadiabatic dynamics: Nonadiabatic derivative couplings and diabatic electronic couplings. *Acc. Chem. Res.* **2015**, *48*, 1340–1350.
- (44) Curchod, B. F. E., Martínez, T. J. Ab initio nonadiabatic quantum molecular dynamics. *Chem. Rev.* **2018**, *118*, 3305–3336.
- (45) Crespo-Otero, R.; Barbatti, M. Recent advances and perspectives on nonadiabatic mixed quantum-classical dynamics. *Chem. Rev.* **2018**, *118*, 7026–7068.
- (46) Nelson, T. R.; White, A. J.; Bjorgaard, J. A.; Sifain, A. E.; Zhang, Y.; Nebgen, B.; Fernandez-Alberti, S.; Mozyrsky, D.; Roitberg, A. E.; Tretiak, S. Non-adiabatic excited-state molecular dynamics: Theory and applications or modeling photophysics in extended molecular materials. *Chem. Rev.* **2020**, *120*, 2215–2287.
- (47) Subotnik, J. E.; Jain, A.; Landry, B.; Petit, A.; Ouyang, W.; Bellonzi, N. Understanding the surface hopping view of electronic transitions and decoherence. *Annu. Rev. Phys. Chem.* **2016**, *67*, 387–417.
- (48) Jain, A.; Alguire, E.; Subotnik, J. E. An efficient, augmented surface hopping algorithm that includes decoherence for use in large-scale simulations. *J. Chem. Theory Comput.* **2016**, *12*, 5256–5268.
- (49) Ohio Supercomputer Center. http://osc.edu/ark:/19495/f5s1ph73 (accessed July 21, 2020).